Journal of Marine Science and Technology

Volume 19 | Issue 5 Article 14

SPACE-TIME LEAST-SQUARES FINITE-ELEMENT METHOD FOR SHALLOW-WATER EQUATIONS

Shin-Jye Liang
Department of Marine Environmental Informatics, National Taiwan Ocean University, No. 2, Beining Road, Keelung, Taiwan, R.O.C., sjliang@ntou.edu.tw

Ying-Chih Chen
Department of Marine Environmental Informatics, National Taiwan Ocean University, No. 2, Beining Road, Keelung, Taiwan, R.O.C.

SPACE-TIME LEAST-SQUARES FINITE-ELEMENT METHOD FOR SHALLOW-WATER EQUATIONS

Acknowledgements

The author would like to thank the National Science Council of Taiwan for financial support (Project no.: NSC 98-2625- M-019-002).

SPACE-TIME LEAST-SQUARES FINITE-ELEMENT METHOD FOR SHALLOW-WATER EQUATIONS

Shin-Jye Liang* and Ying-Chih Chen*

Key words: shallow-water equations, space-time least-squares finite-element method, source terms, standing wave, wave-cylinder interactions.

ABSTRACT

In this paper, a space-time least-squares finite-element method for the 2D nonlinear shallow-water equations (SWE) is developed. The method can easily handle complex geometry, bed slope (source term), and radiation boundary condition without any special treatment. Other advantages of the method include: high order approximations in space and time can easily be employed, no upwind scheme is needed, as well as the resulting system equations is symmetric and positive-definite, therefore, can be solved efficiently with the pre-conditioned conjugate gradient method. The model is applied to several benchmark tests, including standing wave in a flat closed basin, propagation of sinusoidal wave in a flat channel with open boundary, flow past an elliptic hump, and wave-cylinder interactions. Simulation of standing wave in a closed flat basin, with water depth ranging from shallow water to deep water, shows that prediction of SWE model is accurate for shallow waters but inaccurate for deep waters due to the hydrostatic pressure and non-dispersive assumption. Computation of propagation of sinusoidal wave in a flat channel shows open boundary condition is treated satisfactorily. Simulation of flow past an elliptical hump shows good conservation property, and complicate and detailed fine wave structures which were not observed using the low order approximations in previous study. Computed result of wave-cylinder interactions compare well with other numerical results.

I. INTRODUCTION

The depth-averaged, 2D shallow-water equations (SWE) has wide range applications in ocean, environmental and hydraulic engineering, such as, tidal flows in estuary and coastal regions, and open-channel flows in rivers and reservoirs. SWE is a system of nonlinear hyperbolic conservation laws that admits sharp gradient solutions like shock waves and expansion fans. Extensive numerical research has been performed in the area of SWE, such as the finite-difference methods [1], finite-volume methods [4, 8, 23], finite-element methods [10, 15, 17], Godunov-type method [3, 12], and lattice Boltzmann method [42]. And several upwind schemes originally designed to solve the Euler equations in gas dynamics have been extended to the SWE. Some examples are the Roe's method [5], the Beam-Warming scheme, the monotonic upstream schemes for the conservation laws (MUSCL), the Osher and Salmon, the essentially non-oscillatory (ENO) schemes [39, 40], as well as the Harten, Lax and van Leer (HLL) solver. Most of these methods determine the flux vector based on the wave propagation structure, therefore, have the ability of shock capturing with a high level of accuracy [22, 31, 35, 36].

Numerical solution of SWE has been a challenging task because of its nonlinear nature and the need to satisfy the *C*-property. The presence of source terms in momentum equations, such as the bottom slope and friction of bed, compounds the difficulties further. Conservation laws with source terms often have steady-state in which flux gradients are nonzero but exactly balanced by source terms [6, 22, 37]. Many numerical methods (e.g., fractional step methods) have difficulty to preserve such steady-state (the *C*-property) and cannot accurately calculate small perturbations of such state. Numerical solution of SWE with source terms faces problem that low-accuracy solvers yield quite inaccurate solutions, in particular large errors for the wave speed [1]. LeVeque [23] developed a treatment for the bed slope source terms which balanced the source terms and flux gradients. This method is suitable for quasi-steady problems, but is reported to be less successful when applied to calculate steady trans-critical flow with a shock. Zhou, *et al*. [43] proposed the surface gradient method (SGM) for treating source terms in SWE. This method works well for flows with small and mild changes, and experiences difficulty to maintain the conservation property and exhibits numerical oscillations for flows with large changes [31].

Least-squares finite-element method (LSFEM) for approximating the solution of boundary value problems of partial differential equations has been studied at least three decades [11, 16, 19]. In recent years, LSFEMs have been receiving increasing attention in both engineering and mathematics communities. In the engineering literature, for solving Stokes and Na-

Paper submitted 11/05/10; revised 03/21/11; accepted 04/08/11. Author for correspondence: Shin-Jye Liang (e-mail: sjliang@ntou.edu.tw).
**Department of Marine Environmental Informatics, National Taiwan Ocean University, No. 2, Beining Road, Keelung, Taiwan, R.O.C.*

vier-Stokes equations by LSFEMs, the L_2 LSFEMs are the most popular one because L_2 LSFEMs exhibit theoretical and computational advantages in algorithmic design and implementation [7, 11, 16, 19]. One main advantage of LSFEMs is that a single approximating space can be used for all variables [16, 19], and its choice of approximating space is not subject to the Ladyzhenskaya-Babuska-Brezzi (LBB) condition [13, 16]; The other advantage is that resulting system of equations is symmetric and positive-definite (SPD), therefore, can be solved efficiently with the preconditioned conjugate gradient method [9].

LSFEM for SWE using finite-element in space and θ – method in time integration has been studied previously [26, 27]. In this paper, the method is extended using space-time finiteelement approach. The paper is organized as follows. Governing equations and numerical method are presented in Section 2 and 3, respectively. In Section 4, the model is applied to some benchmark problems. Computed results are compared with exact solutions or other numerical results. Based on the computed results, some conclusions are made in Section 5.

II. GOVERNING EQUATION

The depth-averaged, 2D shallow-water equations (SWE) is derived from equation of 2D mass and momentum conservation based on assumption of incompressibility of water, hydrostatic pressure distribution, and a sufficiently small channel slope [20, 28, 38]. The 2D SWE expressed in a non-conservative form reads

$$\begin{cases} \eta_t + [u(h+\eta)]_x + [v(h+\eta)]_y = 0 \\ u_t + uu_x + vu_y + g\eta_x = \nu_t(u_{xx} + u_{yx}) \\ v_t + uv_x + vv_y + g\eta_y = \nu_t(v_{xy} + v_{yy}) \end{cases} \tag{1}$$

where η = free surface elevation; h = water depth; u and v are depth-averaged velocity component in x- and y-coordinate, respectively; ν_t = turbulent kinematic viscosity. ν_t is an important parameter to flow characteristics and practical flow simulations. Relevant reference of ν_t can be found in Yulistiyanto *et al*. [41].

III. NUMERICAL METHOD

Eq. (1) is first linearized with the simple substitution method

$$\begin{cases} \eta_t + \tilde{u}\eta_x + \tilde{v}\eta_y + h_x u + (h+\tilde{\eta})u_x + h_y v + (h+\tilde{\eta})v_y = 0 \\ g\eta_x + u_t + \tilde{u}u_x + \tilde{v}u_y = \nu_t(u_{xx} + u_{yx}) \\ g\eta_y + v_t + \tilde{u}v_x + \tilde{v}v_y = \nu_t(v_{xy} + v_{yy}) \end{cases} \tag{2}$$

where "~" represents value of previous time step. The space-time least-squares finite-element method [18, 32-34] is used, where unknowns (η, u, v) are approximated by

$$\begin{Bmatrix} \eta \\ u \\ v \end{Bmatrix} = \left[M(x,y)N(t)\right] \begin{Bmatrix} \eta^h \\ u^h \\ v^h \end{Bmatrix} \tag{3}$$

where (η^h, u^h, v^h) are the approximations at the nodal point, and $M(x, y)$ and $N(t)$ are the interpolation functions of space-time element. Substitute the approximations, Eq. (3), into governing equations, Eq. (2), one obtain the residuals

$$\begin{Bmatrix} R_h \\ R_u \\ R_v \end{Bmatrix} = \begin{bmatrix} MN_2' + (\tilde{u}M_x + \tilde{v}M_y)N_2 & (\tilde{h}_x M + (h+\tilde{h})M_x)N_2 & (\tilde{h}_y M + (h+\tilde{h})M_y)N_2 \\ gM_x N_2 & MN_2' + (\tilde{u}M_x + \tilde{v}M_y)N_2 - n_t(M_{xx} + M_{yx}) & 0 \\ gM_y N_2 & 0 & MN_2' + (\tilde{u}M_x + \tilde{v}M_y)N_2 - n_t(M_{xy} + M_{yy}) \end{bmatrix} \begin{Bmatrix} h^{n+1} \\ u^{n+1} \\ v^{n+1} \end{Bmatrix}$$
$$+ \begin{bmatrix} MN_1' + (\tilde{u}M_x + \tilde{v}M_y)N_1 & (\tilde{h}_x M + (h+\tilde{h})M_x)N_1 & (\tilde{h}_y M + (h+\tilde{h})M_y)N_1 \\ gM_x N_1 & MN_1' + (\tilde{u}M_x + \tilde{v}M_y)N_1 - n_t(M_{xx} + M_{yx}) & 0 \\ gM_y N_1 & 0 & MN_1' + (\tilde{u}M_x + \tilde{v}M_y)N_1 - n_t(M_{xy} + M_{yy}) \end{bmatrix} \begin{Bmatrix} h^n \\ u^n \\ v^n \end{Bmatrix} \tag{4}$$

in which superscript "n" and "n + 1" represent value of the current and next time step, respectively, and $\Delta t = t^{n+1} - t^n$. The least-squares functional and its minimization principle are then constructed

$$\text{minimize} \int_{\Omega \times T} R^2 \, d\Omega dt \tag{5}$$

Eq. (5) is equivalent to

$$\int_{\Omega \times T} \left\{\frac{\partial R}{\partial \underset{\sim}{u}}\right\}^T R \, d\Omega dt = 0 \tag{6}$$

where Ω and T are space and time domain considered, and

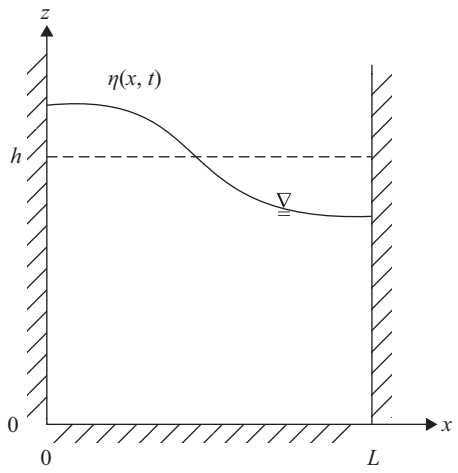

Fig. 1. Illustration of a uni-nodal standing wave in a closed flat channel.

$\underset{\sim}{u} = (\eta^h, u^h, v^h)^{n+1}$. The resulting system of equations is symmetric and positive-definite, therefore, can be solved efficiently by the pre-conditioned conjugate gradient method [9, 19].

IV. COMPUTED RESULTS

The model is applied to following benchmark problems to assess its applicability, conservation property and accuracy. Test cases include (1) standing wave in a flat closed basin, (2) propagation of a sinusoidal wave in a flat channel with open boundary, (3) flow past an elliptical hump, and (4) wave-cylinder interactions. Viscous effect is neglect since its role in the designed problems is not important. All the computations are performed with the linear interpolation in time and 9-node quadrilateral interpolation in space.

1. Standing Wave in a Closed Basin

This problem is designed to test the applicability and conservation property of the model. Standing wave in a flat closed basin is depicted in Fig. 1, where length of the basin L = 10 m (wave length λ = 20 m), water depth h varies, and the initial free surface is

$$\eta(x, 0) = a\cos\left(\frac{\pi x}{L}\right) \tag{7}$$

where a = 0.01 m. Since the basin is closed, boundary condition at both ends is

$$u \cdot n = 0 \tag{8}$$

where n is the outward normal unit vector. A 25 uniform 9-node quadrilateral elements (25 elements in x-direction and 1 element in y-direction) and Δt = 0.5 s is used. Table 1 and Fig. 2 show phase speed at various depth (0.5 ~ 7 m) by the small amplitude wave theory (Airy), shallow-water approximation ($\sqrt{gh}$), shallow-water equations (SWE) model, and Boussinesq equations (BE) model, respectively [25]. For shallow waters (long waves, $h/\lambda \le 1/20$), phase speed of all methods is close. However, as water depth (h) increases, phase speed by SWE model agree well with shallow-water approximation ($\sqrt{gh}$), but differ significantly from phase speed by Airy theory and BE model. This observation supports that applications of SWE model is limited for shallow waters (long waves, $h/\lambda \le 1/20$).

Table 1. Comparison of phase speed of a standing wave in a closed flat basin at various water depth by small amplitude wave theory (Airy), shallow-water approximation ($\sqrt{gh}$), shallow-water equations (SWE) model, and Boussinesq equations (BE) model, respectively [25].

h/L (m)	C_{Airy} (m/s)	$C\sqrt{gh}$ (m/s)	C_{SWE} (m/s)	C_{BE} (m/s)
0.025	2.20456	2.21360	2.40001	2.00200
0.05	3.08056	3.13050	3.20000	3.07692
0.10	4.16797	4.42719	4.39996	4.16667
0.15	4.79272	5.42218	5.60005	4.78469
0.20	5.14970	6.26099	6.40000	5.14139
0.25	5.34883	7.00000	7.19994	5.33333
0.30	5.45788	7.66811	7.71426	5.71428
0.35	5.51691	8.28251	8.28569	5.71428

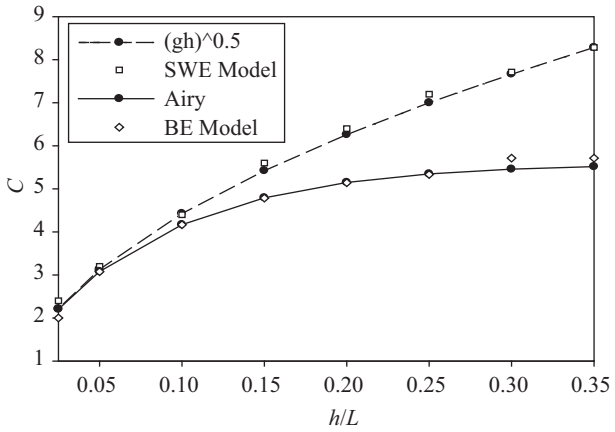

Fig. 2. Comparison of phase speed of a standing wave in a closed flat basin at various water depth by Airy theory, $\sqrt{gh}$, SWE model, and BE model, respectively.

2. Propagation of a Sinusoidal Wave in a Flat Channel with Open Boundary

The problem is designed to test the radiation boundary condition [14, 34]. The computational domain is [0, 20] × [-2.5, 2.5]. At the left boundary, i.e. x = 0, an incident wave is specified

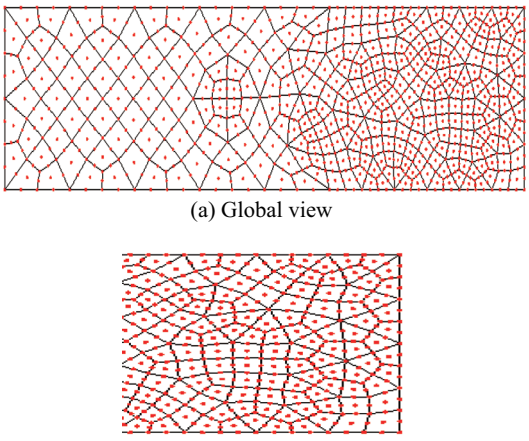

(a) Global view

(b) Zoom in view

Fig. 3. Propagation of sinusoidal wave in a flat channel with open boundary: finite-element meshes of (a) global view and (b) local view near the right exit, respectively.

$$\eta(0, y, t) = a \sin\left(\frac{2\pi t}{T}\right) \tag{9}$$

Where $a = 0.01$ m and $T = 10$ s are the amplitude and period of the incident wave, respectively. At the right boundary, i.e. $x = L = 20$ m, the radiation boundary condition is specified

$$\frac{\partial \eta}{\partial t} + c_x \frac{\partial \eta}{\partial x} + c_y \frac{\partial \eta}{\partial y} = 0 \tag{10}$$

where c_x and c_y are phase speed of propagating wave in the x- and y-direction, respectively, which can be determined by the linear dispersion relation. Still water (h) and gravity acceleration (g) are assumed to be 1 m and 1 m/s^2, respectively. Fig. 3 depicts the computational elements used, 312 9-node quadrilateral elements, where fine elements are concentrated in the right open boundary region. $\Delta t = 0.5$ *s* is used in the computations. Simulation starts with the still water condition. Fig. 4 illustrates the time history of η and u at the middle of exit boundary, ie. $(x, y) = (20, 0)$. As it is shown, wave propagates with wave speed closes to $c = \sqrt{gh} = 1$ m/s, and arrives the right boundary at about $t = 20$ s ($2T$). After a period of transition about $3T$, wave field reaches sinusoidal - Both η and u are sinusoidal with a small distortion. Fig. 5 depicts water surface at various instances. Wave propagates with constant speed to the right and exits freely with unnoticeable reflection. This ensures that the radiation boundary condition, Eq. (10), is modeled satisfactorily.

3. Flow Past an Elliptical Hump

Numerical solution of SWE including source terms is difficult to preserve the steady-state (C-property) and cannot accurately calculate small perturbations of such state. Low-accuracy solvers yield quite inaccurate solutions, in particular

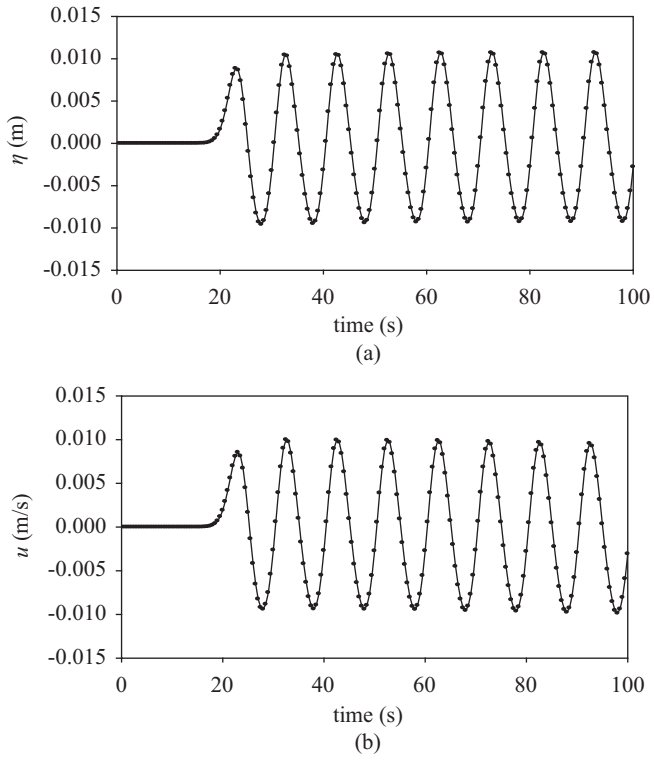

Fig. 4. Propagation of sinusoidal wave in a flat channel with open boundary: Time history of of (a) η and (b) u at the middle of exit boundary, respectively.

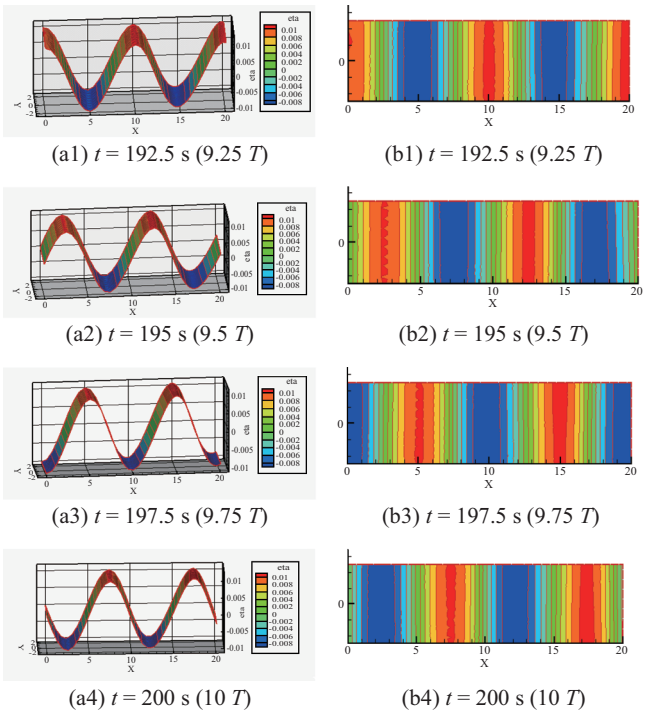

(a1) t = 192.5 s (9.25 T) (b1) t = 192.5 s (9.25 T)

(a2) t = 195 s (9.5 T) (b2) t = 195 s (9.5 T)

(a3) t = 197.5 s (9.75 T) (b3) t = 197.5 s (9.75 T)

(a4) t = 200 s (10 T) (b4) t = 200 s (10 T)

Fig. 5. Propagation of sinusoidal wave in a flat channel with open boundary: (a) 3D view of the water surface (left), and (b) 2D contours of the water surface (right) at t = 9.25 T, 9.5 T, 9.75 T, and 10 T, respectively.

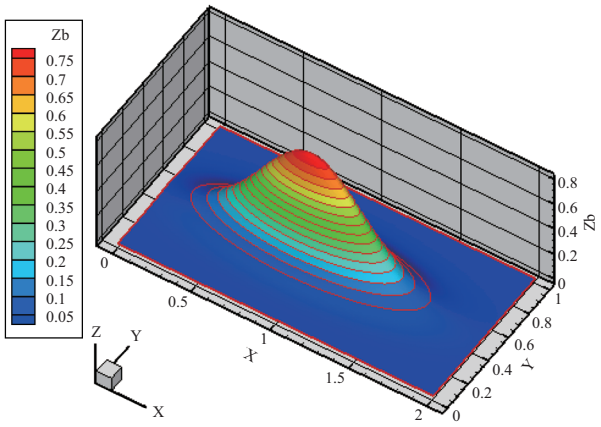

Fig. 6. Flow past an elliptical hump: Illustration of the computational domain and the elliptical shaped hump.

large errors for the wave speed [1]. A widely used benchmark case of the literature [23, 39, 40] is re-examined. The computational domain is $[0, 2] \times [0, 1]$, and the bottom topography, shown in Fig. 6, is given by

$$z(x, y) = 0.8\exp(-5(x-0.9)^2 - 50(y-0.5)^2) \qquad (11)$$

After performing refinement of mesh resolution and time increment, a 200×100 uniform 9-node quadrilateral elements, i.e., $\Delta x = \Delta y = 0.01\ m$ and $\Delta t = 0.001\ s$ are used for computations. First, we consider simulation with the flow at rest initially, i.e. $h = 1$ m and $\eta = 0$ m. We found the exact C-property is respected for a long period of simulation. Then we consider the initial condition with water surface perturbed by the upward displacement 0.01 m in the region $0.05 \le x \le 0.15$

$$\eta(x, y, 0) = \begin{cases} 0.01\ m & \text{if } 0.05 \le x \le 0.15 \\ 0\ m & \text{otherwise} \end{cases} \qquad (12a)$$

The initial momentum in the x and y direction is zero:

$$u = v = 0 m/s \qquad (12b)$$

Fig. 7 shows the 3D contours of free surface and the associated velocity field at various time instances. The initial perturbation propagates to right and is affected by the bottom; It propagates and exits the left boundary with unnoticeable reflection. Shoaling effect (increasing the amplitude of wave due to the decreasing of water depth) is obvious at $t = 0.24\ s$. The wave speed is slower above the hump (due to the shallow water depth) than elsewhere, leading to a distortion of the initially planar perturbation. Standing waves due to the reflection of the hump behind the wave tail is observed at $t =$ 0.24, 0.36, 0.48, and 0.6 s, respectively. These fine detailed wave structures were not observed in Liang and Hsu [26] and Akoh, *et al*. [2, 23]. Reflections and interactions of the surface waves result in complex and symmetric wave structures.

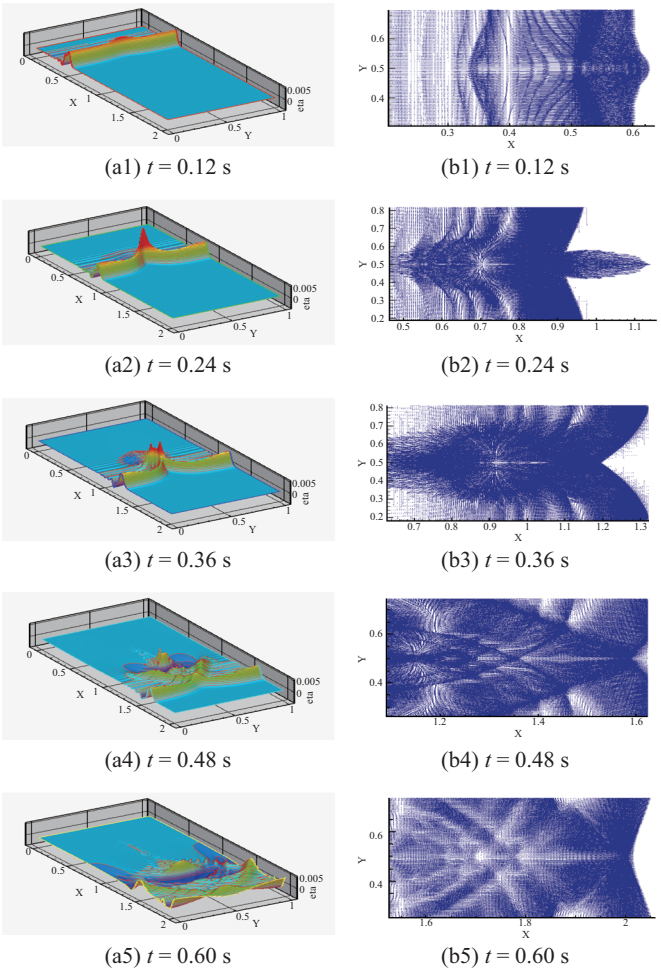

Fig. 7. Wave past an elliptical hump: (a) 3D contours of the water surface and (b) local velocity field at $t = 0.12, 0.24, 0.36, 0.48$, and 0.6 s, respectively.

Fig. 8 shows comparison of the computed water surface of the present study ($\Delta x = \Delta y = 0.01\ m$, and $\Delta t = 0.001\ s$) with the numerical result of Liang and Hsu [26] ($\Delta x = \Delta y = 0.01\ m$, and $\Delta t = 0.0005\ s$) and Akoh, *et al*. [2] ($\Delta x = \Delta y = 0.01\ m$, and $\Delta t = 0.0005\ s$). A 30 uniformly spaced contour lines of water surface level η at t = 0.12, 0.24, 0.36, 0.48, and 0.6 s, respectively, are depicted. Computed water surface contours of Liang and Hsu [26] agrees well with that of Akoh, *et al*. [2]. However, the present method employing a high-order approximation is apparently better to resolve the fine, symmetric wave structures. Overall, predictions of the present model give sharper gradients and detailed wave structures than the numerical results of Liang and Hsu [26] and Akoh, *et al*. [2, 23].

4. Wave-Cylinder Interactions

Wave past a circular cylinder in a flat channel is studied numerically in [24] and Liang and Hsu [26]. Computational domain is $[0, 6.4] \times [0, 3.2]$. The cylinder is located in the center of the consider domain with radius $r = 0.25\ m$. The

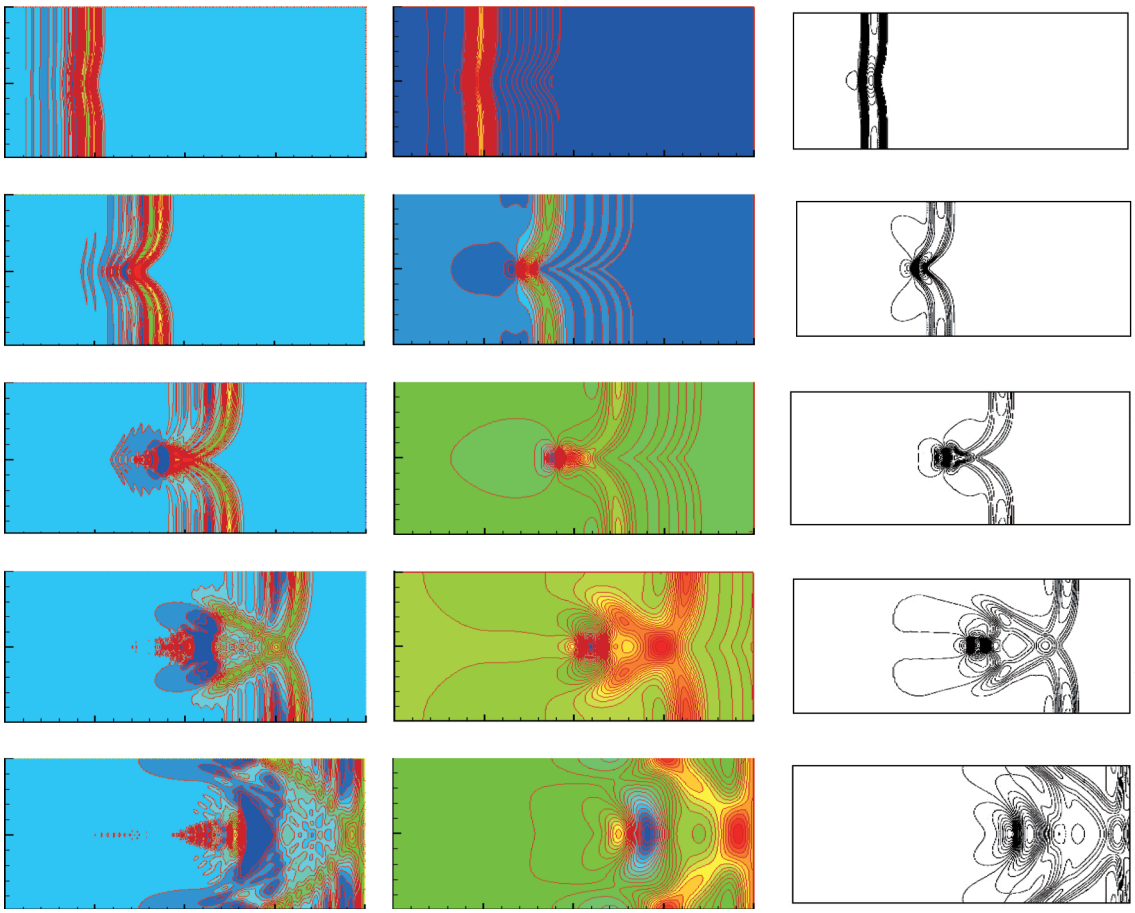

Fig. 8. Wave past an elliptical hump: 2D contours of the water surface of (a) present study with 9-node quadrilateral elements (left), and (b) results of Liang and Hsu [26] with 3-node triangular meshes (middle), and (c) result of Akoh, *et al.* [2] (right) at t = 0.12, 0.24, 0.36, 0.48, and 0.6 s, respectively.

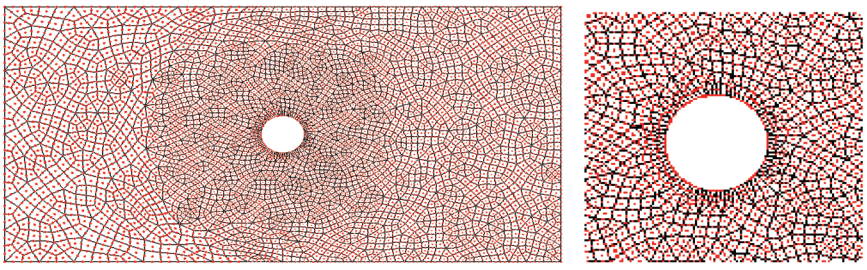

Fig. 9. Wave-cylinder interactions: finite-element meshes of (a) global view and (b) local view near the cylinder, respectively.

undisturbed water depth is h = 0.12 m, resulting in ka = 1.0, where k is wave number and a is wave amplitude, respectively. A 14,292 nodes and 5,518 9-node quadrilateral elements, depicted in Fig. 9, and Δt = 0.052 s is used for simulation. Radiation boundary condition, i.e. $\partial\eta/\partial t + c_x\partial\eta/\partial x = 0$, is specified at the right open boundary. The incident wave with wave amplitude a = 0.00463 m and period T = 1.3 s is enforced at the left boundary. Simulation starts with water at rest initially. Flow reaches a periodic state after a period of transition about 2T.

The 3D perspective and 2D contours of water surface at various time instances of a period is shown Fig. 10. In windward of the cylinder, standing waves present due to the combination of incident and reflected waves, while scattered waves is relatively weak. Reflection and wave runup due to the blockage of the cylinder is obvious. In the lee side of cylinder, scattered waves are relatively weak due to the blockage of the cylinder. Diffractions and wave-cylinder interactions

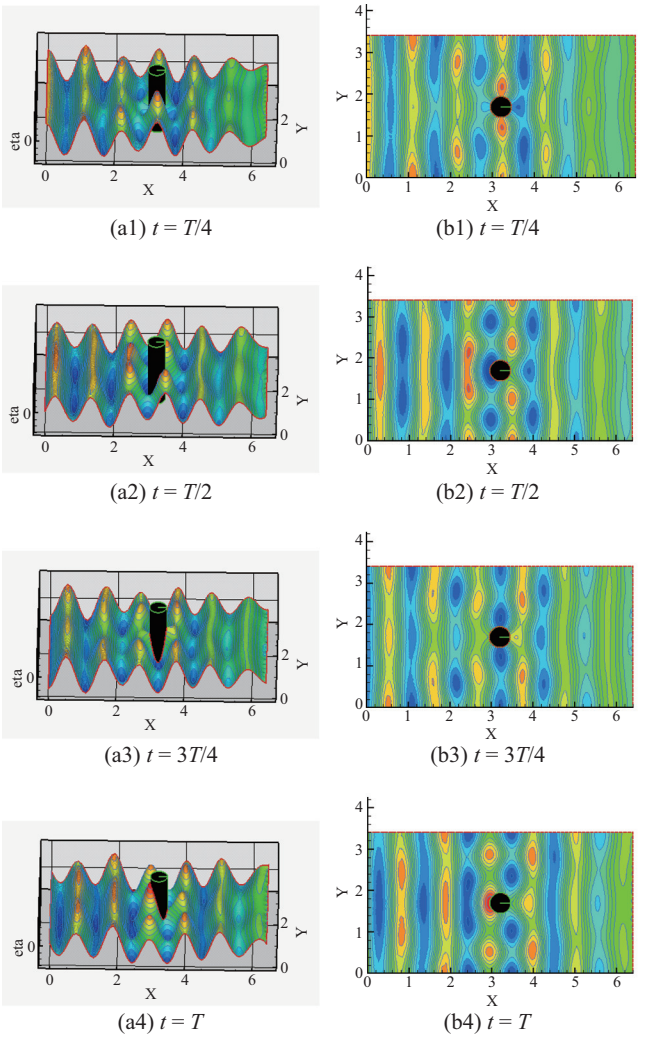

Fig. 10. Wave-cylinder interactions: (a) 3D view of the water surface (left), and (b) 2D contours of the water surface (right) at $t = T/4$, $T/2$, $3T/4$, and T, respectively.

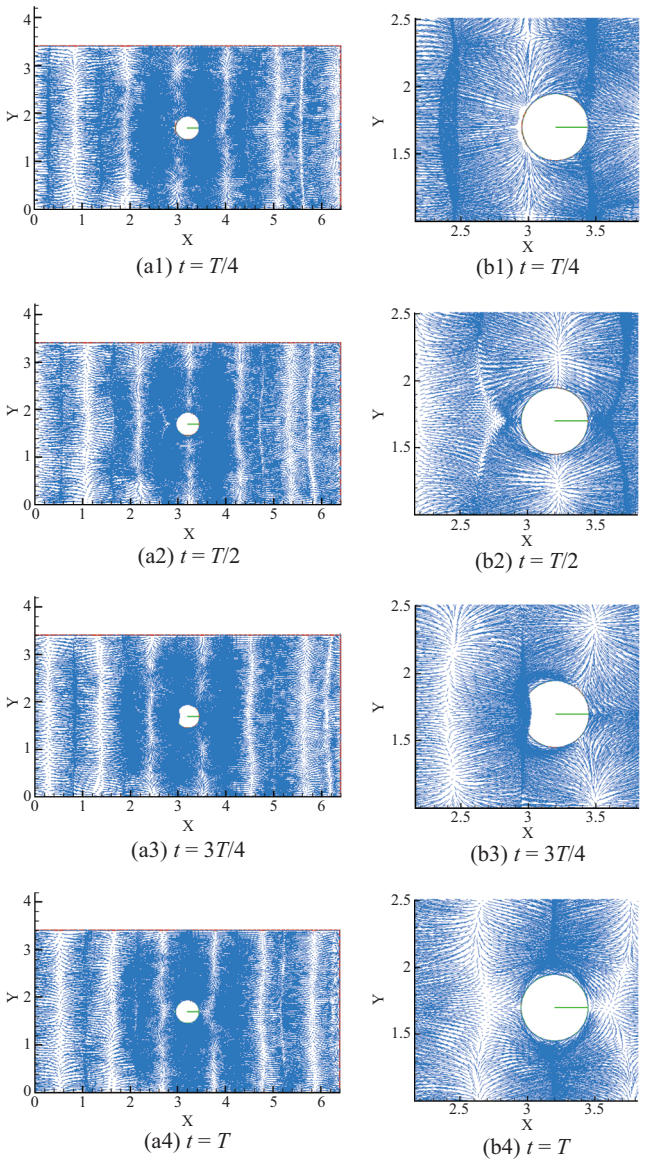

Fig. 11. Wave-cylinder interactions: (a) Global view of the velocity field (left), and (b) local view of the velocity field (right) at $t = T/4$, $T/2$, $3T/4$, and T, respectively.

result in complex and symmetric wave structures, and exit the right boundary with unnoticeable reflection. These results are very close to the results of previous study using a 29,982 nodes and 59,196 3-node triangular elements, and $\Delta t = 0.01$ *s* [26]. The corresponding velocity field is depicted in Fig. 11. At $t = T/4$, free surface starts to fall and reflected velocity is strong in windward of the cylinder since free surface and velocity is out of phase. At $t = T/2$, wave trough hits the cylinder front and velocity is weak in t of the cylinder. At $t = 3T/4$, free surface starts to rise and incoming velocity reaches the maximum. At $t = T$, wave crest hits the cylinder front and velocity is weak again. The wave field repeats itself periodically.

ACKNOWLEDGMENTS

The author would like to thank the National Science Council of Taiwan for financial support (Project no.: NSC 98-2625-M-019-002).

REFERENCES

1. Abbot, M. B., Damsgaard, A., and Rodenhuis, G. S., "SYSTEM 21, Jupiter, A design system for two-dimensional nearly horizontal flows," *Journal of Hydraulic Research*, Vol. 11, pp. 1-28 (1973).
2. Akoh, R., Ii, S., and Xiao, F., "A CIP/multi-moment finite volume method for shallow water equations with source terms," *International Journal for Numerical Methods in Fluids*, Vol. 56, pp. 2245-2270 (2008).
3. Alcrudo, F. and Garcia-Navarro, P., "A high resolution Godunov-type scheme in finite volume for the 2D shallow water equation," *International Journal for Numerical Methods in Fluids*, Vol. 16, pp. 489-505 (1993).
4. Alessandro, V., Caleffi, V., and Zanni, A., "Case study: Malpasset dam-break simulation using a two-dimensional finite volume method," *ASCE Journal of Hydraulic Engineering*, Vol. 128, pp. 460-472 (2002).
5. Ambrosi, D., "Approximation of shallow water equations by Roe's Reimann solver," *International Journal for Numerical Methods in Fluids*,

Vol. 20, pp. 157-168 (1995).
6. Bermudez, A. and Vazquez, M. E., "Upwind methods for hyperbolic conservation laws with source terms," *Computers & Fluids*, Vol. 23, pp. 1049-1071 (1994).
7. Bochev, P. B. and Gunzburger, M. D., "Finite element methods of least-squares type," *SIAM Review*, Vol. 40, pp. 789-837 (1998).
8. Burguette, J. and Garcia-Navarro, P., "Efficient construction of high-resolution TVD conservative schemes for equations with source terms: Application to shallow water flows," *International Journal for Numerical Methods in Fluids*, Vol. 37, pp. 209-248 (2001).
9. Carey, G. F. and Jiang, B. N., "Element-by-element linear and nonlinear solution scheme," *Communications in Applied Numerical Methods*, Vol. 2, pp. 145-153 (1986).
10. Cheng, R. T., "Modeling of hydraulic systems by finite element methods," *Advances in Hydroscience*, Vol. 11, pp. 207-284, Academic Press (1978).
11. Deang, J. M. and Gunzburger, M. D., "Issues related to least-squares finite element methods for the Stokes equations," *SIAM Journal on Scientific Computing*, Vol. 20, pp. 878-906 (1998).
12. Fujihara, M. and Borthwick, A. G. L., "Godunov-type solution of curvilinear shallow-water equations," *ASCE Journal of Hydraulic Engineering*, Vol. 126, pp. 827-836 (2000).
13. Girault, V. and Raviart, P., *Finite Element Methods for Navier-Stokes Equations: Theory and Algorithm*, Springer (1986).
14. Givoli, D., "Non-reflecting boundary conditions, a review," *Journal of Computational Physics*, Vol. 94, pp. 1-29 (1991).
15. Gracia, R. and Kahawita, R. A., "Numerical solution of the St. Venant equations with the MacCormack finite element scheme," *International Journal for Numerical Methods in Fluids*, Vol. 6, pp. 507-527 (1986).
16. Gunzburger, M. D., *Finite Element Methods for Viscous Incompressible Flows*, Academic Press (1989).
17. Hervouet, J.-M., *Hydrodynamics of Free Surface Flows: Modelling with the Finite Element Method*, John Wiley & Sons (2007).
18. Hughes, T. J. R. and Hulbert, G. M., "Space-time finite element methods for elastodynamics: Formulations and error estimates," *Computer Methods in Applied Mechanics and Engineering*, Vol. 66, pp. 339-363 (1988).
19. Jiang, B. N., *The Least-Squares Finite Element Method*, Springer (1998).
20. Johnson, R. S., *A Modern Introduction to the Mathematical Theory of Water Waves*, Cambridge (1997).
21. Laibel, J. P. and Pinder, G. F., "Solution of the shallow water equations by least squares collocation," *Water Resources Research*, Vol. 29, pp. 445-455 (1993).
22. LeVeque, R. J., *Numerical Methods for Conservation Laws*, Birkhauser-Verlag (1990).
23. LeVeque, R. J., "Balancing source terms and flux gradients in high-resolution Godnov methods: the quasi-steady wave-propagation algorithm," *Journal of Computational Physics*, Vol. 146, pp. 346-365 (1998).
24. Li, Y. S. and Zhan, J. M., "Boussinesq-type model with boundary-fitted coordinate system," *Journal of Waterway, Port, Coastal, and Ocean Engineering*, Vol. 127, pp. 152-160 (2001).
25. Liang, S.-J. and Chen, Y.-C., "Comparison of numerical solution of shallow-water equations and Boussinesq equations for standing wave in a closed basin," *Proceedings of 32nd Ocean Engineering Conference in Taiwan*, Keelung, Taiwan (2010). (in Chinese)
26. Liang, S.-J. and Hsu, T.-W., "Least-squares finite-element method for shallow-water equations with source terms," *Acta Mechanica Sinica*, Vol. 25, pp. 523-532 (2009).
27. Liang, S.-J., Tang, J.-H., and Wu, M.-S., "Solution of shallow-water equations using least-squares finite-element method," *Acta Mechanica Sinica*, Vol. 24, pp. 523-532 (2008).
28. Mei, C. C., Stiassnie, M., and Yue, D. K.-P., Theory and Applications of Ocean Surface Waves, I: Linear Aspects & II: Nonlinear Aspects, World Scientific (2005).
29. Nwogu, O., "An alternative form of the Boussinesq equations for modeling the propagation of waves from deep to shallow water," ASCE *Journal of Waterways, Port, Coastal and Ocean Engineering*, Vol. 119, pp. 618-638 (1993).
30. Peregrine, D. H., "Long waves on a beach," *Journal of Fluid Mechanics*, Vol. 27, pp. 815-827 (1967).
31. Rebollo, T. C., Delgado, A. D., and Nieto, E. D. F., "A family of stable numerical solvers for the shallow water equations with source terms," *Computer Methods in Applied Mechanics and Engineering*, Vol. 192, pp. 203-225 (2003).
32. Tezduyar, T. E., Behr, M., Mittal, S., and Liou, J., "A new strategy for finite element computations involving moving boundaries and interfaces – The deforming-spatial-domain/space-time procedure: II. Computation of free-surface flows, two-liquid flows, and flows with drifting cylinders," *Computer Methods in Applied Mechanics and Engineering*, Vol. 94, pp. 353-371 (1992).
33. Thompson, L. L. and Pinsky, P. M., "A space-time finite element method for structural acoustics in infinite domains, part I: Formulation, stability, and convergence," *Computer Methods in Applied Mechanics and Engineering*, Vol. 132, pp. 195-227 (1996).
34. Thompson, L. L. and Pinsky, P. M., "A space-time finite element method for structural acoustics in infinite domains, part II: Exact time-dependent non-reflecting boundary conditions," *Computer Methods in Applied Mechanics and Engineering*, Vol. 132, pp. 229-258 (1996).
35. Toro, E. F., *Reimann Solvers and Numerical Methods for Fluid Dynamics*, Springer-Verlag (1997).
36. Toro, E. F., *Shock-Capturing Methods for Free-Surface Shallow Flows*, John Wiley & Sons (2001).
37. Vazquez-Cendon, M. E., "Improved treatment of source terms in upwind schemes for the shallow water equations in channel with irregular geometry," *Journal of Computational Physics*, Vol. 148, pp. 497-526 (1999).
38. Whitham, G. B., *Linear and Nonlinear Waves*, Wiley-Interscience (1999).
39. Xing, Y. and Shu, C. W., "High order finite difference WENO schemes for a class of hyperbolic systems with source terms," *Journal of Computational Physics*, Vol. 208, pp. 206-227 (2005).
40. Xing, Y. and Shu, C. W., "High order well-balanced finite volume WENO schemes and discontinuous Galerkin methods for a class of hyperbolic systems with source terms," *Journal of Computational Physics*, Vol. 214, pp. 567-598 (2006).
41. Yulistiyanto, B., Zech, Y., and Graf, W. H., "Flow around a cylinder: Shallow-water equations modeling with diffusion-dispersion," *Journal of Hydraulic Engineering, ASCE*, Vol. 124, pp. 419-429 (1998).
42. Zhou, J. G., "A lattice Boltzmann model for the shallow water equations," *Computer Methods in Applied Mechanics and Engineering*, Vol. 191, pp. 3527-3539 (2002).
43. Zhou, J. G., Causon, D. M., Mingham, C. G., and Ingram, D. M., "The surface gradient method for the treatment of source terms in the shallow-water equations," *Journal of Computational Physics*, Vol. 168, pp. 1-25 (2001).